metals

MDPI

Article

Effect of Al Addition on Martensitic Transformation Stability and Microstructural and Mechanical Properties of CuZr Based Shape Memory Alloys

Carlo Alberto Biffi [1,*], Jacopo Fiocchi [1], Mauro Coduri [2] and Ausonio Tuissi [1]

[1] National Research Council, Institute of Condensed Matter Chemistry and Technologies for Energy, Via Previati 1/E, 23900 Lecco, Italy; jacopo.fiocchi@icmate.cnr.it (J.F.); ausonio.tuissi@cnr.it (A.T.)
[2] Department of Chemistry, University of Pavia, Viale Taramelli 16, 27100 Pavia, Italy; codurimauro@gmail.com
* Correspondence: carloalberto.biffi@cnr.it

Abstract: In this work, the effect of the Al content (x = 5, 10, and 15 at. %) on the martensitic transformation (MT) and microstructure and mechanical properties of $Cu_{(50-x)}Zr_{50}Al_x$ alloys was studied. The microstructure of the alloys was characterized at room temperature by means of scanning electron microscopy and X-ray diffraction. An increase in Al content reduces the amount of transforming CuZr phase, and consequently the secondary phase formation is favored. The evolution of the MT upon thermal cycling was investigated as a function of the Al content by differential scanning calorimetry. MT temperatures and enthalpies were found to be decreased when increasing the Al content. Al addition can induce a sudden, stable MT below 0 °C, while the binary alloy requires ten complete thermal cycles to stabilize. Finally, the mechanical properties were investigated through microhardness and compression testing. No linear dependence was found with composition. Hardness lowering effect was observed for 5–10 at. % of Al content, while the hardness was increased only for 15 at. % Al addition with respect to the binary alloy. Similarly, compressive response of the alloys showed behavior dependent on the Al content. Up to 10 at. % Al addition, the alloys indicate a superelastic response at room temperature, while higher Al content induced untimely failure.

Keywords: shape memory alloys; intermetallic; microstructure; differential scanning calorimetry; X-ray diffraction; mechanical testing

Citation: Biffi, C.A.; Fiocchi, J.; Coduri, M.; Tuissi, A. Effect of Al Addition on Martensitic Transformation Stability and Microstructural and Mechanical Properties of CuZr Based Shape Memory Alloys. *Metals* **2021**, *11*, 1141. https://doi.org/10.3390/met11071141

Academic Editors: Sergey Kustov and Alexander V. Shelyakov

Received: 17 May 2021
Accepted: 1 July 2021
Published: 20 July 2021

1. Introduction

In recent years, worldwide interest has spurred on great efforts in the development of shape memory alloys (SMAs) to be applied for automotive, aerospace, mechanical, and control systems [1]. Among the SMAs, the near-equiatomic NiTi compound is the most applied for industrial applications, as it shows stable and performing functional properties [1,2]. Other SMA systems, even Ni and Ti free ones, have been investigated in the literature because of the possibility of offering performances with limited costs within different operating temperature ranges. Among these, the intermetallic CuZr has been studied extensively, since it exhibits a reversible, non-thermoelastic martensitic transformation (MT) above 100 °C when subjected to thermal cycles. The literature offers some studies reporting investigations into the microstructure and functional properties of both CuZr [3–9] and CuZr based shape memory alloys [10–18].

At first, Firstov et al. reported that equiatomic, intermetallic CuZr shows a MT below 140 °C [3] from the parent austenite (A) phase (cubic B2, space group Pm-3m), stable at high temperature, into two martensitic phases (M) with monoclinic structure (space groups Cm and *P*21/*m*) [4,5]. This system can show secondary phases, Cu10Zr7 and CuZr2, as reported by Carvalho et al. [6].

Biffi et al. showed that the characteristic temperatures of the MT at the first thermal cycle and the Cu/Zr ratio in quasi-equiatomic composition are strongly correlated [7]. It

was reported that the equiatomic composition appears to be the best compromise between the greatest amount of material involved in the MT and the highest transformation temperatures for considering CuZr within high temperature shape memory alloys (HTSMAs). In other studies, it was found that upon thermal cycling the initial MT, present at the first thermal cycle, is suppressed, and a new one, stable at temperatures below 0 °C and with limited thermal hysteresis, takes its place [8–10]. Electrical resistivity measurements showed a large shift of the characteristic temperatures, followed, after tens of thermal cycles, by a new type of MT at approximately −10 °C [8]. Moreover, thermal cycling through differential scanning calorimetry evidenced this new MT, from austenite to a new martensitic structure, which was different than the original one present in the first few cycles [9,10].

In yet another study, it was found that a B2 CuZr solid-phase transformation can exist at a high temperature [11]. The CuZr-based alloys were classified into three different types, related to the precipitation and stability of the B2 phase. An innovative way based on a prediction strategy for the formation of different sized CuZr-based shape memory bulk metallic glass composites (BMGC) was proposed for evaluating the competition among the vitrification, the precipitation of metastable B2 CuZr, and room-temperature equilibrium phases.

Due to this lack of stability during phase transformations, as well as to improve the alloys' workability, efforts have been made to study the addition of several alloying elements, like Co, Cr, Ni, Al, and Ti [10–16].

It was found that Co addition has a stabilizing effect on the MT temperatures during thermal cycling [10–14], while Ni addition can shift the MT to higher temperatures above 200 °C but weakens the shape memory effect [10–13,15].

Hot workability can also be improved by the addition of Ni and Co together, while Ti alloying does not confer any evident benefits to Cu-Zr systems and reduces the transformation temperatures [16,17]. Other alloying elements, like Cr and Al, generally decrease the characteristic temperatures of the MT [14,18–23]. In particular, the effect of Al addition up to 15 at. % in place of Cu was studied [18–22]: it was found that the transformation temperatures of the ternary alloys were decreased with respect to the binary one at the first thermal cycle [20].

In the present work, the effect of Al addition to CuZr based SMAs is investigated in terms of the evolution of the MT upon thermal cycling. A comparison with the equiatomic alloy, thermally cycled for stabilizing the MT [9], was made in order to define the principal differences among the binary and ternary systems. The study was carried out through differential scanning calorimetry (DSC) for measuring the characteristic temperature of the MT. Scanning electron microscopy (SEM) with energy dispersion spectroscopy (EDS) and θ–2θ X-ray Diffraction analysis (XRD), all at room temperature, were proposed for the microstructural analysis. Mechanical properties were evaluated using microhardness measurements and compression testing, which were also done at room temperature.

2. Experimental

Pure metals Zr, Al, and OFHC grade Cu were melted by means of a vacuum arc furnace (Leybold mod. LK 6/45) with a non-consumable tungsten electrode to obtain small cylindrical buttons (30 mm in diameter and about 40 g in weight). The melting furnace was equipped with a water-cooled copper crucible to avoid contamination of the liquid pool; the melting was done in a high purity inert atmosphere (Ar 99.99% at 400 mbar pressure). The nominal atomic compositions of the chosen alloy were the following: $Cu_{(50-x)}Zr_{50}Al_x$ with x = 0, 5, 10, 15 at. %. The produced buttons were re-melted six times, being flipped over after each melting step in order to ensure high homogeneity in their composition. After melting, the specimens were fully annealed at 850 °C for 3 h under Ar atmosphere (800 mbar) with final quenching in water at room temperature for homogenizing the microstructure of the small ingots. The water quench allows us to perform uniform cooling in the entire sample. The grain size was evaluated to be around 100–200 μm.

The microstructure of the alloys was observed by means of scanning electron microscopy (SEM Leo 1413, Carl Zeiss AG, Jena, Germany) using back scattered electrons (BSE); quantitative analysis of the secondary phases was performed by means of energy dispersive X-ray spectroscopy (EDS), calibrated with a Co reference. Diffraction data (CuKα, λ = 1.5418 Å) were collected on a θ:2θ vertical scan Panalytical X'Pert PRO diffractometer (Malvern Panalytical Ltd, UK), equipped with parallel (Soller) slits—0.04 rad—and a real time multiple strip detector. The generator was operated at 40 kV and 30 mA; slits were used with a divergence of 0.5°. The scans were performed in the 25–55° 2θ range at 25 °C on bulk specimens. The goal of the XRD analysis is to identify the phases present. Since the specimens are textured, we used Rietveld refinements, applying corrections for preferred orientation, to verify that the intensities were reliable. Once the phases involved were defined, lattice parameters were obtained by Le Bail refinements.

The calorimetric analysis was carried out on fully annealed samples using a differential scanning calorimeter (mod. SSC 5200 by Seiko Instruments, Chiba, Japan) at a rate of 10 °C/min; heating/cooling scans were performed at temperatures ranging from −100 °C to 450 °C for a number of 10 thermal cycles. Characteristic temperatures and the corresponding transformation heats were evaluated for both direct/reverse transformations upon cooling/heating scans, respectively. Microhardness measurements were performed on the cross section of the samples using a Future Tech Corporation FM-700 hardness tester (Future-Tech Corp FM-700, Tokyo, Japan), applying a 200 g load for 15 s. Compressive tests were conducted at room temperature by means of an MTS 2/M machine (MTS Systems Corporation, Eden Prairie, MN, USA), equipped with extensometer, at a strain rate of 0.015 min^{-1}; five complete cycles, loading and unloading up to 1% in strain, were carried out on cylindrical samples (3 mm in diameter and 8 mm in height).

3. Results and Discussion

SEM images of the samples and related EDS analyses are shown in Figure 1 and Table 1, respectively. The binary $Cu_{50}Zr_{50}$ alloy (see Figure 1a) appears to consist of a CuZr matrix containing the secondary phase $Cu_{10}Zr_7$. This result is consistent with previous work [7,9,14,24].

Table 1. EDS measurements of the CuZr based sample, performed on the sites depicted in Figure 5.

Composition	Phases	Measured Compositions (at. %)
$Cu_{50}Zr_{50}$ (see Figure 1a)	(1) CuZr	$Cu_{47}Zr_{53}$
	(2) $Cu_{10}Zr_7$	$Cu_{61}Zr_{39}$
$Cu_{45}Zr_{50}Al_5$ (see Figure 1b)	(1) CuZr	$Al_{5.5}Cu_{46}Zr_{48.5}$
	(2) τ5	$Al_{18}Cu_{42}Zr_{40}$
	(3) $O_x(CuZr_2)$	$Al_{12}Cu_{31}Zr_{46}O_{11}$
$Cu_{40}Zr_{50}Al_{10}$ (see Figure 1c)	(1) CuZr	$Al_6Cu_{45}Zr_{49}$
	(2) τ5	$Al_{21}Cu_{41}Zr_{38}$
	(3) $CuZr_2$	$Al_4Cu_{35}Zr_{61}$
	(4) $O_x(CuZr_2)$	$Al_{16}Cu_{28}Zr_{44}O_{12}$
$Cu_{35}Zr_{50}Al_{15}$ (see Figure 1d)	(1) CuZr	$Al_{5.5}Cu_{46,5}Zr_{48}$
	(2) τ5	$Al_{23}Cu_{40}Zr_{37}$
	(3) $CuZr_2$	$Al_5Cu_{37}Zr_{58}$
	(4) $O_x(CuZr_2)$	$Al_{17}Cu_{30}Zr_{46}O_7$

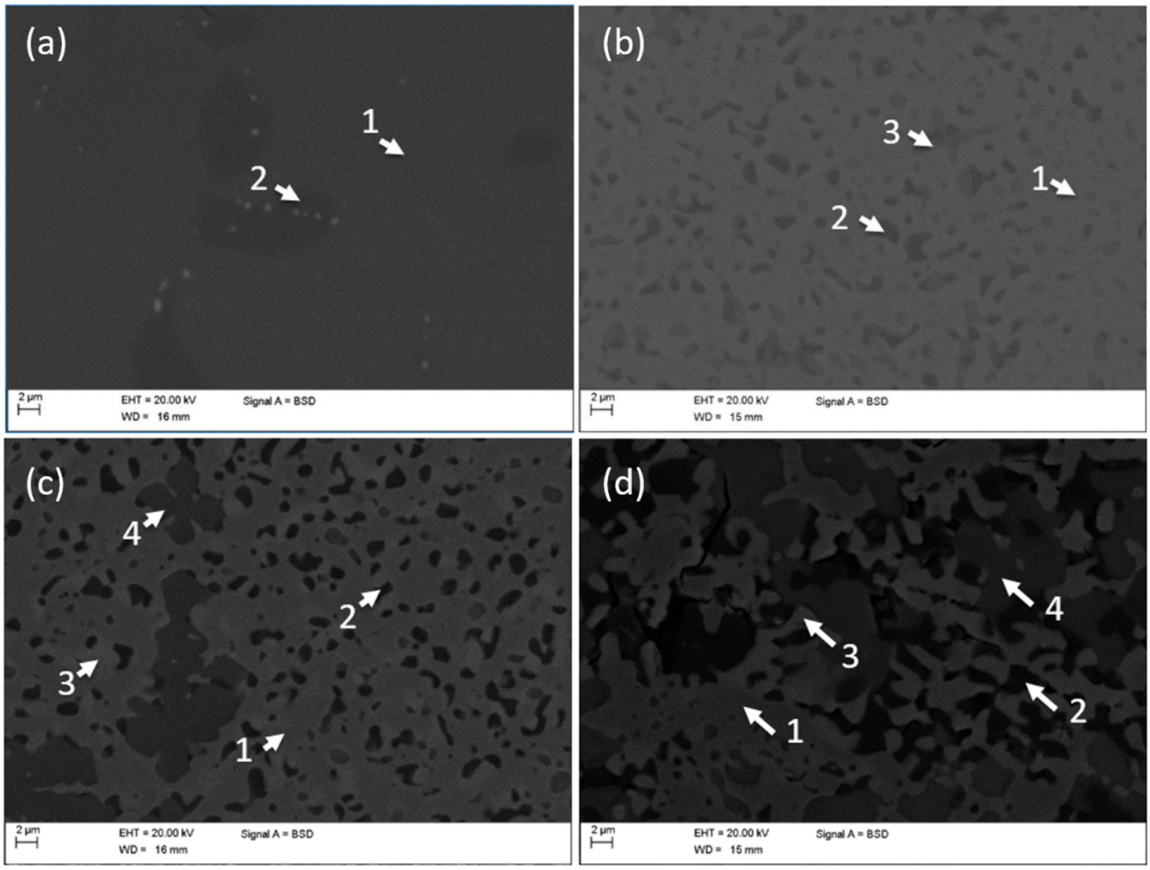

Figure 1. BSE-SEM images of $Cu_{50}Zr_{50}$ after MT stabilization (**a**) and $Cu_{(50-x)}Zr_{50}Al_x$ with x = 5, 10, 15 at. % (**b**–**d**) before thermal cycling, respectively.

Figure 1b shows the microstructure of $Cu_{45}Zr_{50}Al_5$. A predominance of the CuZr matrix (light colored area) containing small traces of a ternary phase (dark areas) and some cross-shaped oxides (grey areas) can be seen. As listed in Table 1, the ternary phase exhibits an average composition of Cu_2Zr_2Al. A very similar secondary phase, in terms of morphology and elemental composition, was observed by Meng et al. [20] in samples annealed at the same temperature as in the present investigation. After comparison with XRD analysis, this secondary phase was identified as τ5, although the compositional stability range of the τ5 phase was previously proposed to be limited to $ZrCu_xAl_{2-x}$ with x ranging from 0.34 to 0.95 [24–26].

A further increase in Al content (10 at. %) induced the formation of $CuZr_2$ and an increase in the number of secondary phases (see Figure 1c). Numerous dark regions of τ5, with average composition $Zr_{40}Cu_{42}Al_{18}$ (at. %), are dispersed into the CuZr matrix. Finally, cross-like oxides, characterized by a composition similar to the ones found in $Cu_{45}Zr_{50}Al_5$, were also detected. The brighter areas surrounding τ5 and oxide particles were found to exhibit a composition lying in the range of the $CuZr_2$ phase. In the sample containing 15% Al (see Figure 1d), the high amount of aluminum induced a strong increase in the content of the τ5 phase (dark areas). A high amount of $CuZr_2$, some of which oxidized, was also found. The formation of the $CuZr_2$ oxides, already reported in Cu-Zr system [6], is considered to take place during melting, according to the high oxygen reactivity of Zr, which is similar to that of Ti. It is well known that the oxides inhibit the shape memory behavior in quasi-equiatomic NiTi alloys; in the present system, the influence of these oxides on the MT, although not clear, can probably be considered similar to that of equiatomic NiTi alloys.

A remark is due on the distribution of Al within the different phases. Concerning the CuZr matrix, EDS analysis revealed that the Al content, present as solid solution in the CuZr matrix, is constant: an average content of 5.5%, 6.0%, and 5.5% was found in

$Cu_{(50-x)}Zr_{50}Al_x$ with x = 5, 10, 15 at. %, respectively. These values match those reported by Meng et al. [20] well, who stated that the solubility limit of Al in the CuZr phase is about 5 at. %. Since the CuZr phase is always found to be rich in Zr, it is assumed that Al might preferentially substitute for Cu rather than for Zr. On the other hand, the correct $CuZr_2$ stoichiometry can be guaranteed only by considering that the doping Al substitutes for Zr. This is particularly true as far as the related oxide, which is well known to form cross-like sections with a $CuZr_2O_{0.5}$ base composition, is concerned. In this case, the oxidized areas in samples $Cu_{40}Zr_{50}Al_{10}$ and $Cu_{35}Zr_{50}Al_{15}$ were found to contain a high amount of aluminum, up to 20 at. %. The metallic radius of Al (143 pm), being exactly intermediate between those of Cu and Zr (128 pm and 160 pm [24], respectively) is likely to lie at the basis of this apparently controversial behavior.

Figure 2 displays the experimental XRD patterns of binary and ternary alloys, focusing on the 20 to 50 degrees region, where most of the main peaks occur. Different labels were employed to mark the peaks of the main phases. As reported by Biffi et al. [18], before any thermal cycles the equiatomic binary alloy is composed of the two monoclinic martensites. In addition to these, $Cu_{10}Zr_7$ and $CuZr_2$ secondary phases are present in the Cu/Zr ratio close to 1:1. The blurred features of the pattern confirm that most of the sample is composed of martensites, the contributions of which, being quite close to each other, were not resolved in the indexing, as is generally observed for CuZr compounds [15].

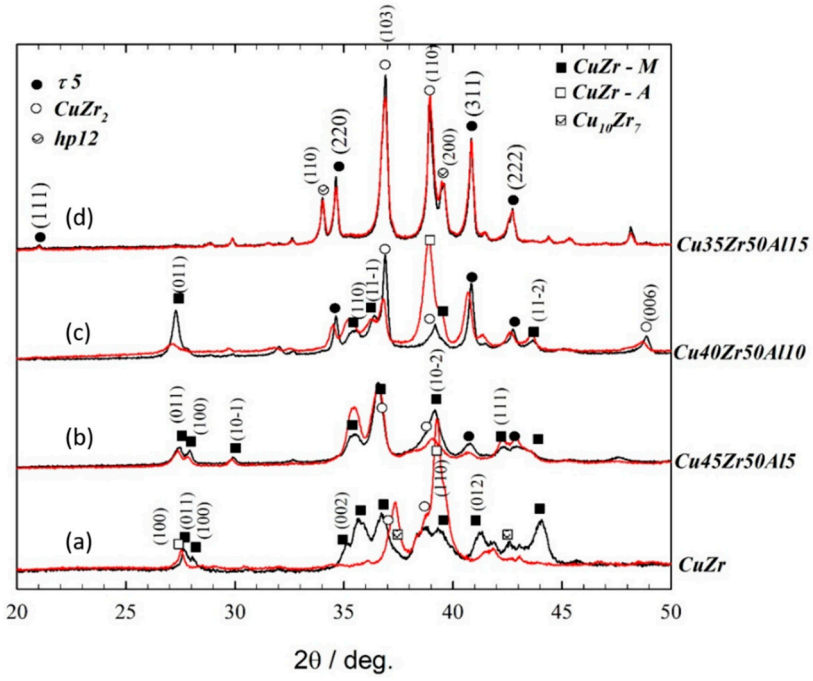

Figure 2. Section of experimental patterns of binary equiatomic (**a**) and ternary alloys (**b**–**d**) at room temperature, before (black curve) and after (red curve) the tenth thermal cycle. The reflections of the τ5 phase are explicitly indicated.

The addition of Al progressively consumes CuZr, in agreement with the decreasing heat exchange from DSC, leading to the preferential growth of two different phases: $CuZr_2$ and τ5. The latter phase can be clearly distinguished since the intensity of its main four reflections, well resolved from other contributions, steeply increases with Al amount. The position and relative intensities of the peaks are consistent with a phase having space group Fd-3m and lattice parameter 7.326 Å. The compositional range of stability of the τ5 phase has then to be reconsidered from that originally proposed in [14,15]. Besides the τ5 phase, Al addition increases the proportion of the $CuZr_2$ phase as well.

The lattice parameters for the main phases of interest are reported in Table 2. The B19′ martensite is actually composed of two phases, however, as the second phase is a

superstructure of the former and most of the reflections are shared, here we consider only the $P2_1/m$ for the sake of simplicity. While the absolute values might be an average of those of the two phases, they can provide information about the lattice response to Al incorporation. The presence of Al shrinks the CuZr lattice parameters, especially axes *a* and *b*. This is consistent with the slight enrichment of Cu in place of Zr, making Al substituting more likely for the latter. Similarly, the incorporation of Al within $CuZr_2$ is confirmed by the evident contraction of the lattice parameter *c*, from 11.20 Å for the binary alloy down to 11.05 Å, which is also consistent with the progressive enrichment of Cu (and depletion of Zr) observed via SEM-EDS. On the other hand, the lattice parameter of the τ5 phase is nearly invariant across the different compositions.

Table 2. Lattice parameters (Å and °) of martensite CuZr ($P2_1/m$) and $CuZr_2$ as a function of Al content. Uncertainties are estimated to be 0.005 Å and 0.2°.

Composition	CuZr				$CuZr_2$	
	a	***b***	***c***	***β***	***a***	***c***
$Cu_{50}Zr_{50}$	3.253	4.394	4.964	105.2	3.253	11.200
$Cu_{45}Zr_{50}Al_5$	3.171	4.433	4.910	104.6	3.219	11.148
$Cu_{40}Zr_{50}Al_{10}$	3.144	4.244	4.920	104.9	3.201	11.166
$Cu_{35}Zr_{50}Al_{15}$	-	-	-	-	3.160	11.045

SEM-EDS analysis indicates that Al shows the tendency of substituting either for Cu or for Zr, depending on the phase of interest. Therefore, increasing the Al amount in $Zr_{50}Cu_{50-x}Al_x$ increases the relative amount of Zr vs. Cu, thus moving towards the Zr-rich part of the phase diagram, i.e., stabilizing the $CuZr_2$ phase. Indeed, we observed the preferential formation of $CuZr_2$ rather than $Cu_{10}Zr_7$ as a secondary phase [27].

Finally, the XRD pattern related to the Al addition of 15 at. % clearly shows the presence of contributions other than CuZr, $CuZr_2$, and τ5. Beside a minor contribution of the τ10 phase, two big reflections at ~34.0° and 39.5° were tentatively indexed with a hexagonal phase (hp12 in Figure 5) related to that of $ZrAl_2$. It cannot be excluded that this phase may be related to the Al-rich oxide observed by SEM-EDS. The different elemental composition between binary and ternary alloys does not only define the nature and amount of the phases; it also drastically affects stability against thermal cycling.

Figure 2 compares the experimental XRD patterns of binary CuZr (see Figure 3a) and ternary CuZrAl alloys with 5, 10 and 15 at. % Al (see Figure 3b–d) before and after 10 thermal cycles across MT. The pattern of the binary alloy is definitely altered upon cycling, owing to both the transformation from fully martensitic to fully austenitic phases and to the increased amount of secondary $Cu_{10}Zr_7$ and $CuZr_2$ phases. It is worth noting that the cycling was performed in the diffractometer, hence the sample position was not altered and all modifications observed in the XRD patterns are ascribable to the structure evolution only. On the other hand, ternary alloys are not significantly modified upon cycling. The two patterns of sample with 15 at. % Al are very similar, testifying that the same phase composition and relative concentration are maintained upon cycling. Only a slight increase in peak broadening was observed, suggesting an accumulation of defects or residual stresses.

DSC scans of stabilized $Cu_{50}Zr_{50}$ and $Cu_{(50-x)}Zr_{50}Al_x$ alloys in fully annealed condition are shown in Figure 3. As previously reported by the authors [9,10], the binary alloy exhibits unstable behavior. The MT temperatures are initially above 100 °C. Upon thermal cycling, they are shifted down to lower temperatures (martensite start temperature, M_s = 150 °C at the first cycle, M_s = −20 °C at the 8th cycle). After the 8th cycle no variation in DSC signals is detected, as depicted in Figure 3a, and the MT shows stable behavior below 0 °C. The stabilized transformation is also characterized by a much narrower thermal hysteresis (less than 10 °C).

It is evident that 5 at. % Al addition promotes MT thermal cycling stability (see Figure 3b). Furthermore, the Al addition suddenly decreases MT transformation temperatures from the very first thermal cycle, as depicted in the DSC scan magnification of Figure 3b–d where a stable MT peak with M_s of −54 °C is visible. The increasing of Al content up to 15 at. % does not affect the thermal stability of the MT but it reduces transformation temperatures as well as DSC signals, as reported in Figure 3c,d, for 10 and 15 at. % of Al, respectively. As displayed in Figure 4a, the addition of 5 at. % Al induces an evident decrease in the transformation temperatures, whereas the further increase towards 10 at. % and 15 at. % of Al causes a more progressive depression of the characteristic temperatures. The enthalpy values associated with forward and reverse phase transformations are reported in Figure 4b as a function of the Al content: the increase of the Al content decreases both enthalpies from about 3 J/g, for the binary alloy, down to 0.5 J/g, for the ternary alloy with 15 at. % Al content. This may be explained by considering that the amount of the phase involved in the MT, i.e., the Al-free Cu-Zr, decreases, as seen for the binary CuZr alloys too [6]. In fact, in this work it was found that the equiatomic phase is associated with the MT, and a shift of the chemistry of the alloy away from the 1:1 Cu to Zr ratio indicates a decrease in the enthalpy involved during the MT. The DSC results are only in partial agreement with the work done by Meng et al. [20]: the shape of the peaks of the MT for all investigated Al contents is slightly different between the literature and the current work. Another significant difference is that the MT occurred at temperatures below 0 °C (see Figure 4), while Meng et al. indicated that the MT occurred at higher temperatures [20]. This was probably due to the grain size and the specific melting system adopted for the sample preparation. Moreover, the current heat treatment was carried out for 3 h while in Meng's work it took 72 h.

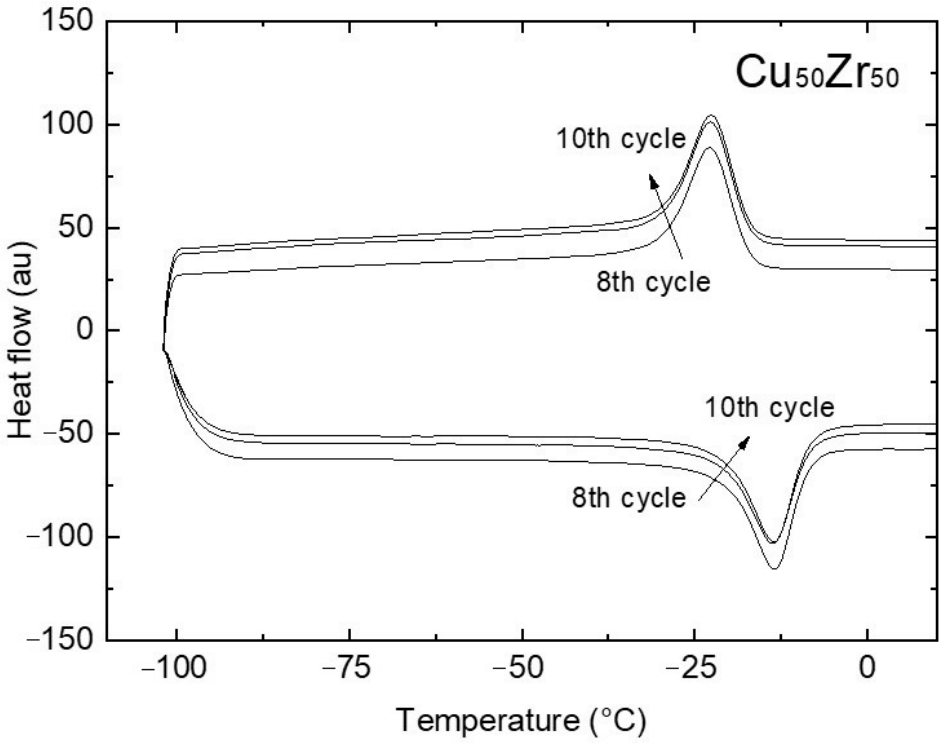

(**a**)

Figure 3. *Cont.*

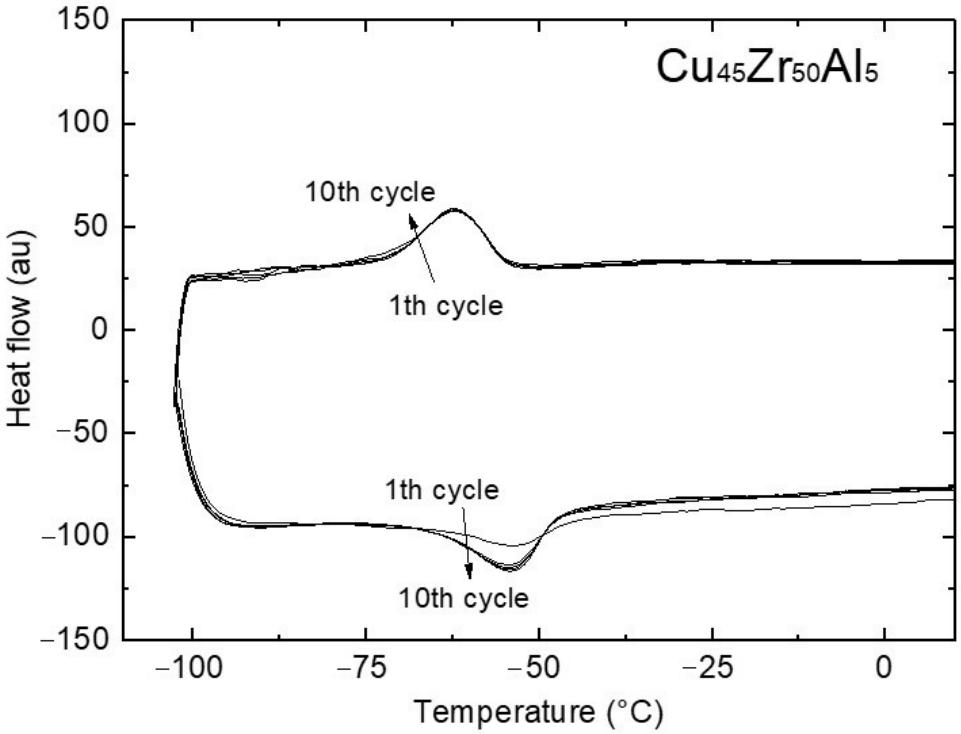

(**b**)

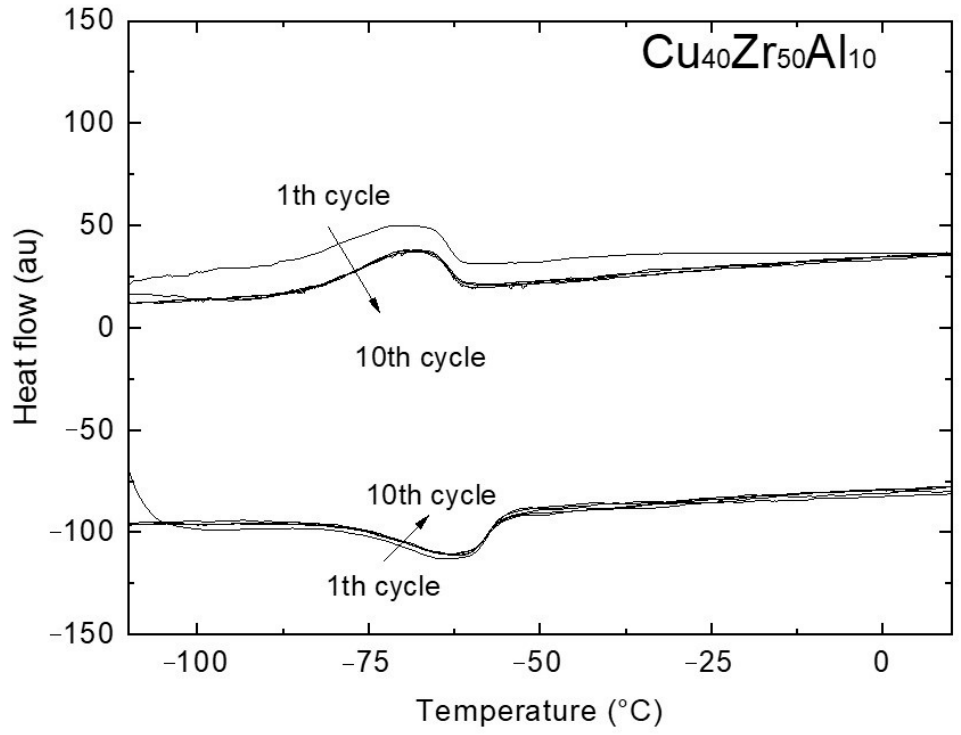

(**c**)

Figure 3. *Cont.*

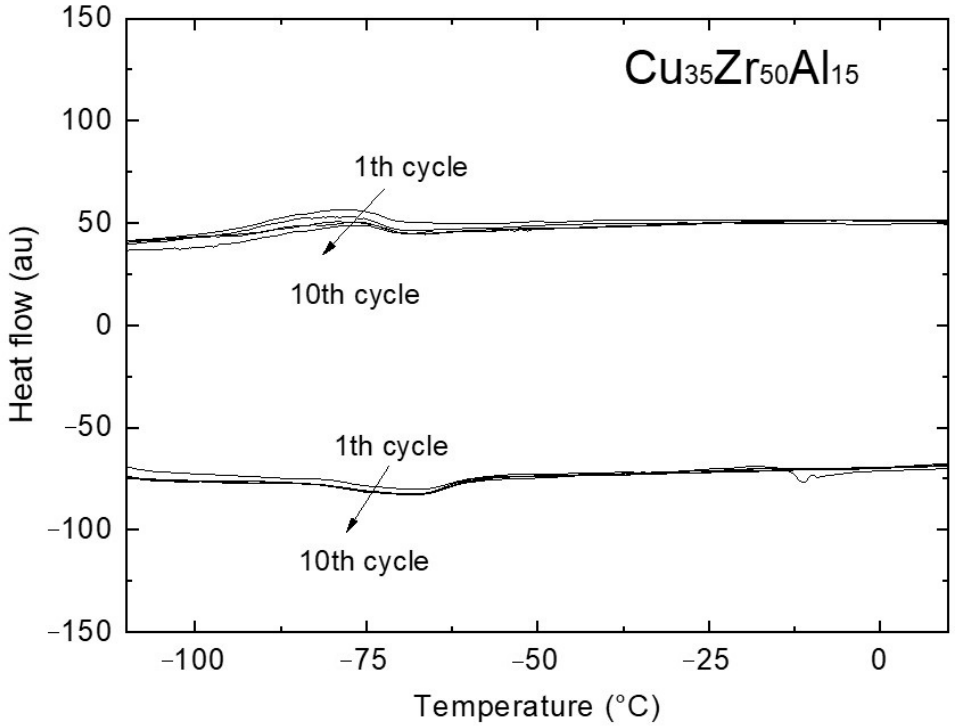

(**d**)

Figure 3. DSC scans of CuZr based alloys: MT after stabilization of $Cu_{50}Zr_{50}$ alloy (**a**); thermal cycling of $Cu_{(50-x)}Zr_{50}Al_x$ alloys with Al = 5, 10, 15 at. % (**b**–**d**), respectively.

Additionally, the thermal hysteresis increases when moving from the equiatomic to the ternary alloys, and it is directly proportional to the Al content, as previously indicated. The transformation enthalpies, which are related to the CuZr phase transformation [7], decrease as Al content increases. This might suggest a lowering of the amount of CuZr phase involved in the MT, as below reported. As shown in Figure 5, the trend of microhardness of the investigated alloys indicates a softening moving from the binary $Cu_{50}Zr_{50}$, having an average hardness of 550 HV, to the ternary alloy with the lowest Al content, having an average hardness of 450 HV. Increasing the Al content from 5 at. % to 10 at. % does not modify the hardness values while moving up to 15 at. % of aluminum induces an increase in the mechanical properties. A similar trend in $(CuZr_2)_{100-x}Al_x$ was observed by Qiu et al. [18]. This trend appears to be in good agreement with the mechanical response of the alloys tested in compression during five complete loading/unloading cycles.

Figure 6 shows the stress/strain curves, obtained at room temperature during quasi-static compression testing, for the stabilized equiatomic CuZr alloy and for the three ternary alloys. Uniaxial compression testing was selected for studying the mechanical response of these alloys, as it has been widely used to study the mechanical properties of materials having a lack of tensile ductility. The trend of the maximum stress, recoverable, and residual strains during mechanical cycling as a function of the Al content are reported in Figure 7.

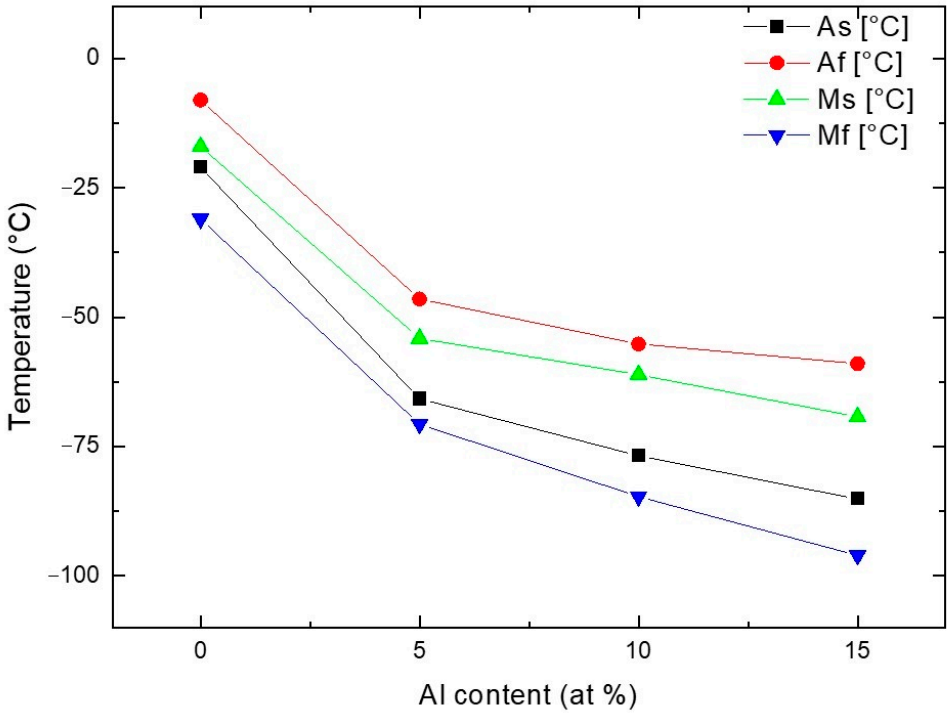

(**a**)

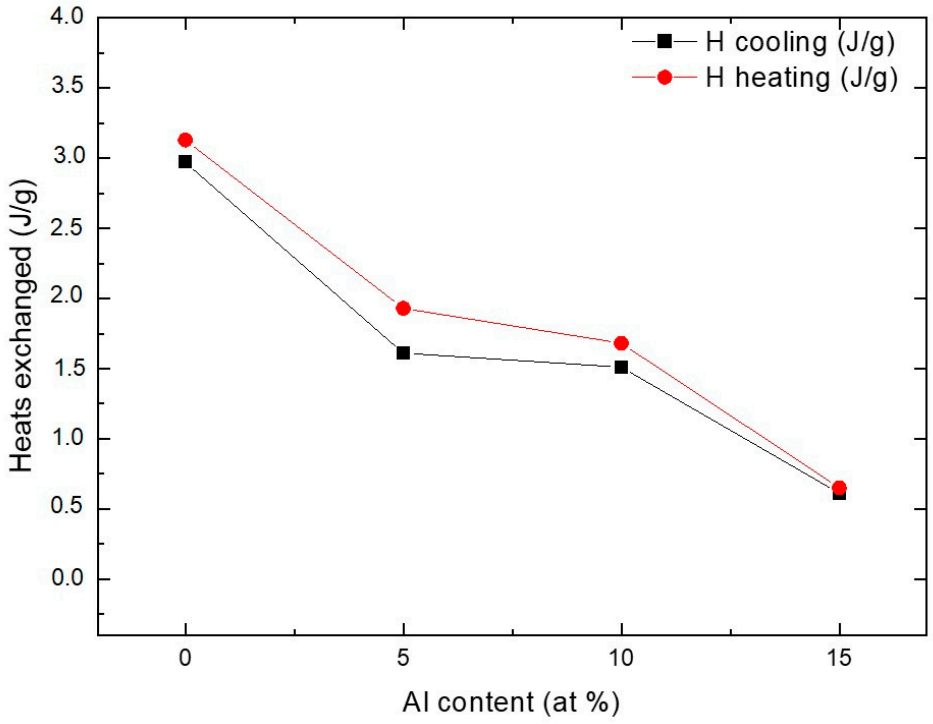

(**b**)

Figure 4. Transformation temperatures (**a**) and heat exchanged (**b**) of $Cu_{(50-x)}Zr_{50}Al_x$ with x = 0, 5, 10, 15 at. % after MT stabilization.

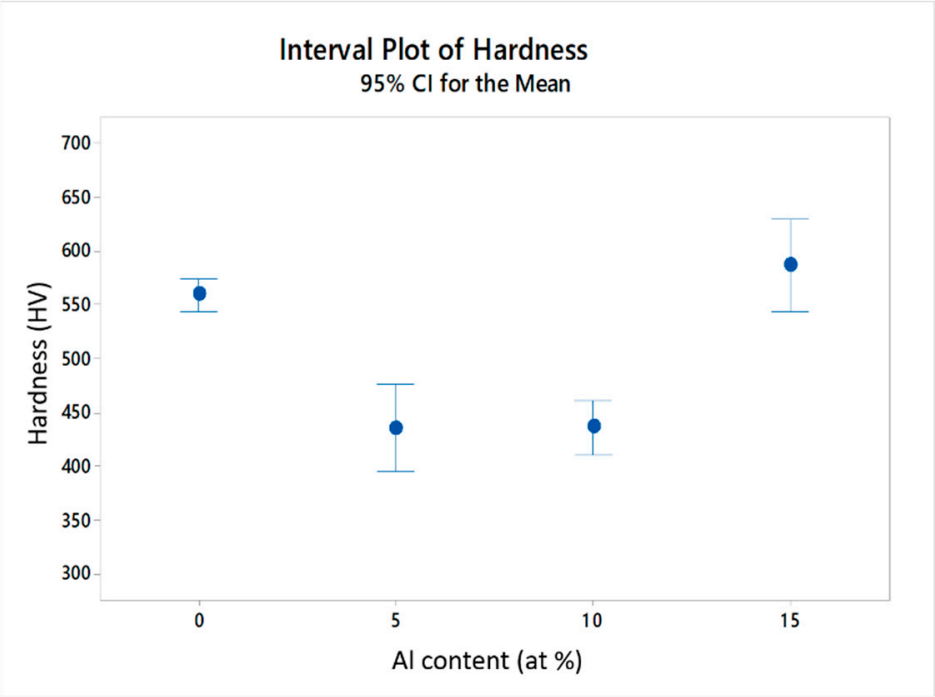

Figure 5. Microhardness as a function of the Al content.

In details, the thermally stabilized binary CuZr alloy shows perfect linear behavior during the first cycle, while the second one exhibits a superelastic behavior with a more than intensive linear strain hardening effect, which is correlated with the high temperature phase (see DSC scan of Figure 3a). This response remains present up to the fifth cycle, during which the failure occurred before reaching the maximum stress during the loading. The addition of Al in the range between 5% and 10% provokes an increase in the values of the recoverable strain during each cycle and the failure cannot be reached within the fifth cycle. The loading and unloading slopes are much lower for these compositions of the ternary system, if compared with the binary alloy. On the contrary, higher Al content clearly induces a brittle response (see Figure 6d), which is supported by an increase in brittleness. The alloy fragility could be correlated with the accumulation of defects or residual stresses, previously detected by the XRD analysis. In fact, the failure of the last composition was found during the loading of the fourth cycle, therefore corresponding to the minor number of mechanical cycles.

As shown in Figure 7a, the maximum stress can be correlated with the Al content similarly to the microhardness values: this behavior indicates that the effect of Al addition on the mechanical properties can be well estimated. As the binary alloy has the highest recoverable strain, its failure occurs in the fifth cycle; similar to the behavior of the alloy with the highest Al content. On the contrary, 5at. % and 10at. % of Al addition promote the best recoverable performances during the mechanical cycling without reaching the failure of the samples up to 2% in correspondence of 0.5% of residual strain (see Figure 7b). The binary CuZr was characterized by the highest value of residual strain, up to 1%. All the ternary alloys were associated with a decrease of the residual strain, indicating an improvement of the elastic behavior, as shown in Figure 7c.

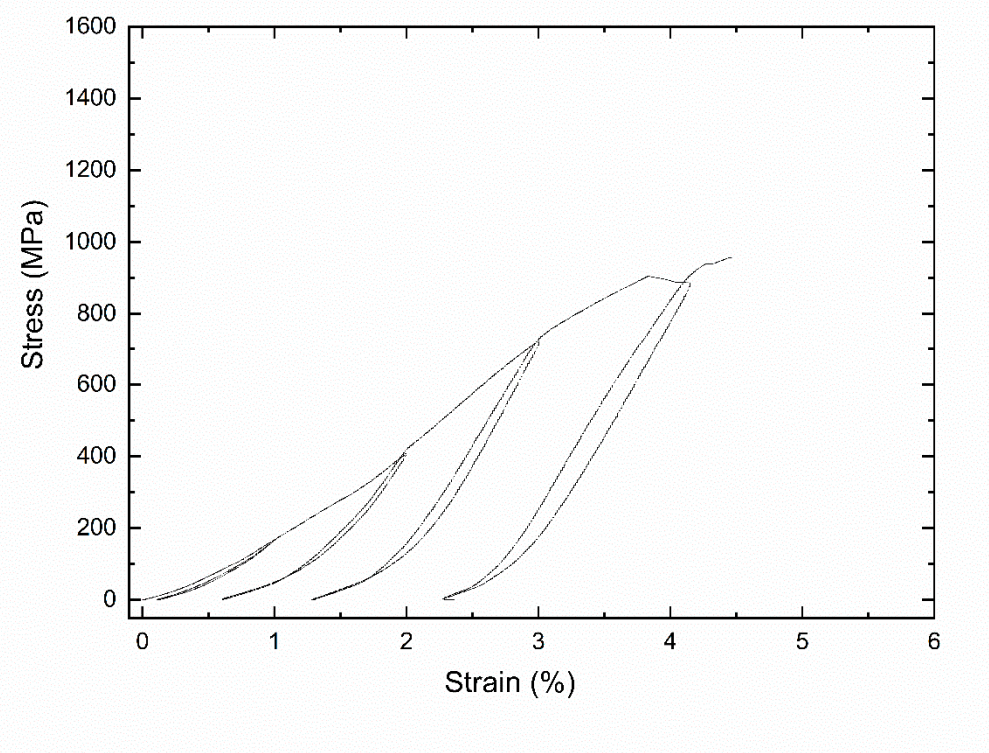

(**a**)

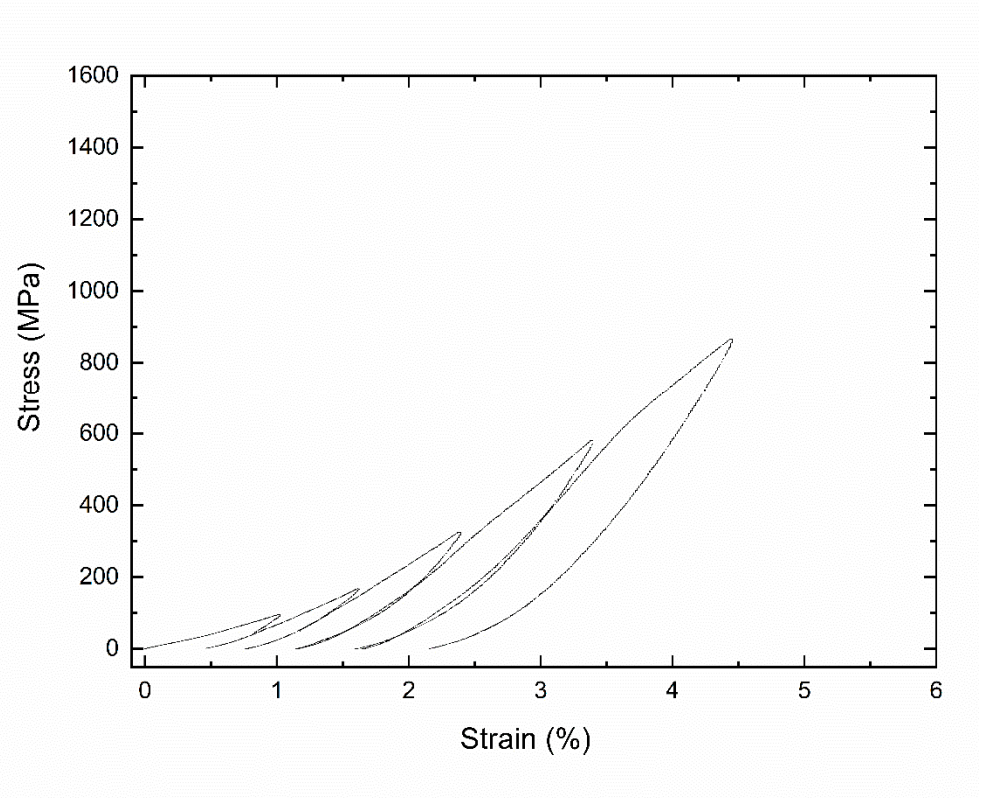

(**b**)

Figure 6. *Cont.*

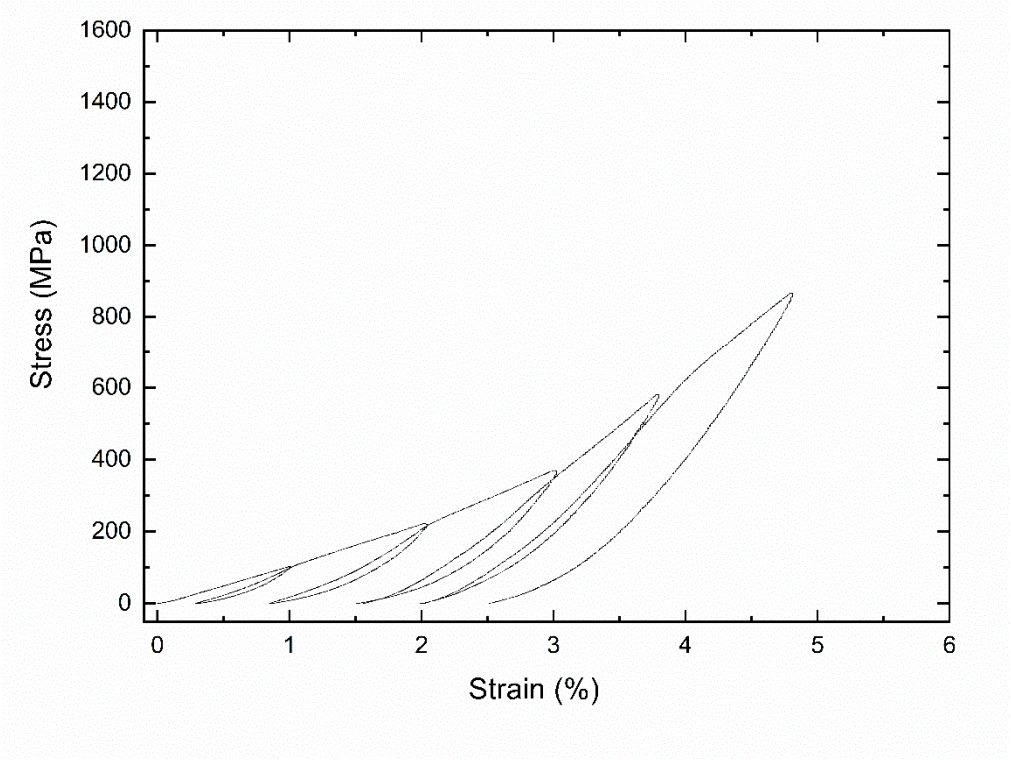

(**c**)

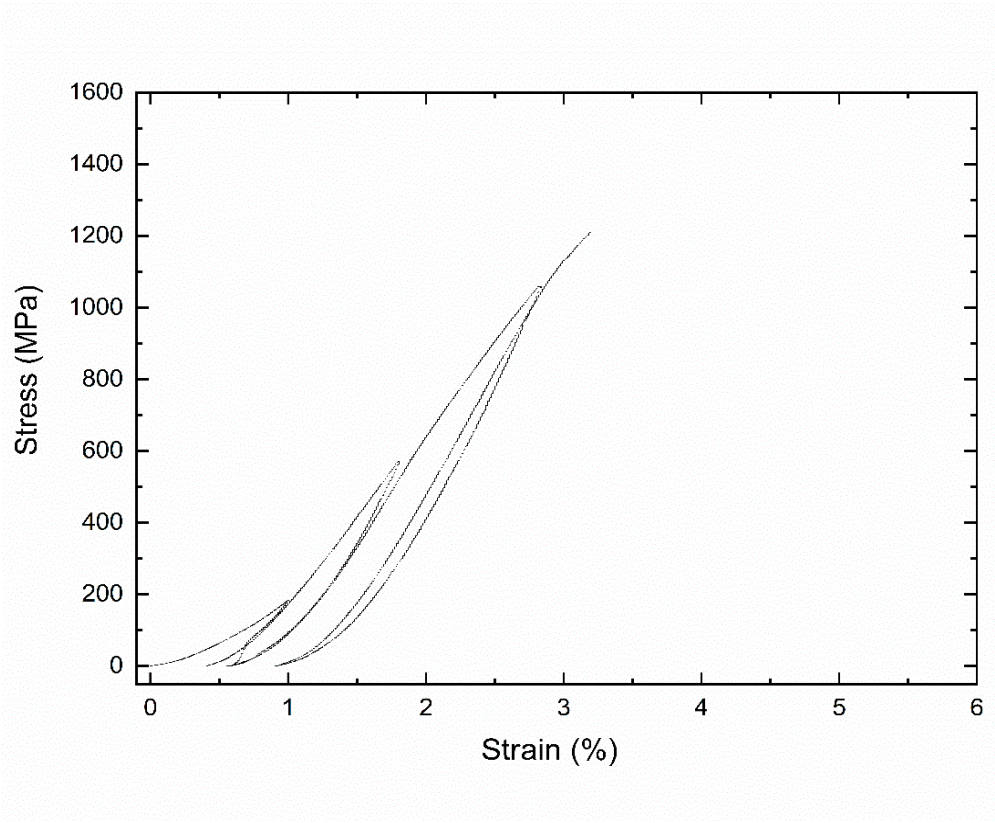

(**d**)

Figure 6. Compression behavior of CuZr based alloys, tested at room temperature: stress–strain after stabilization of $Cu_{50}Zr_{50}$ alloy (**a**); and $Cu_{(50-x)}Zr_{50}Al_x$ alloys with Al = 5, 10, 15 at. % (**b**–**d**), respectively. The stresses and strains are compressive.

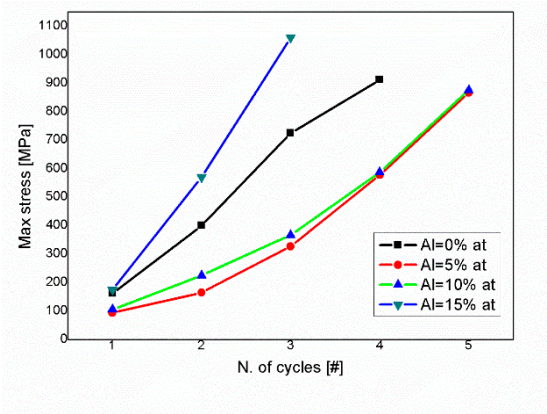

(**a**)

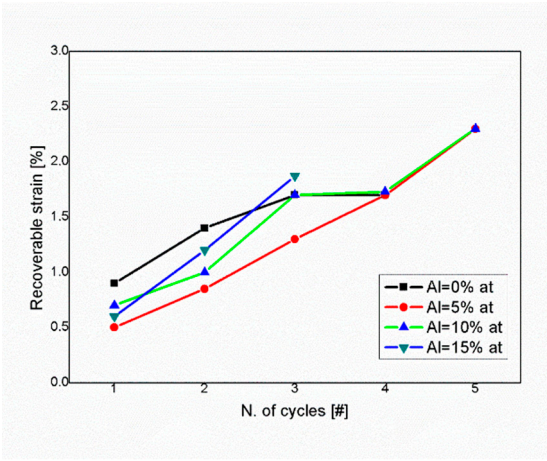

(**b**)

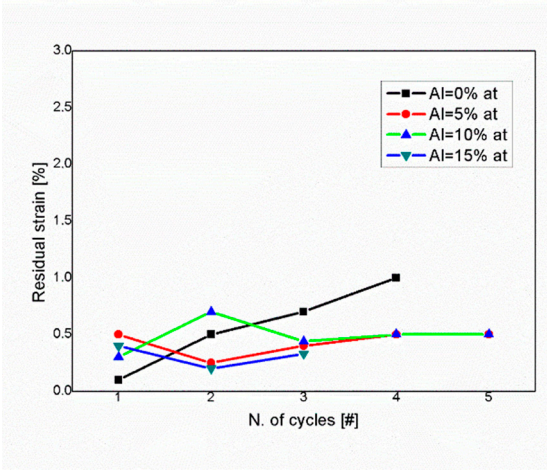

(**c**)

Figure 7. Trend of maximum stress (**a**), recoverable (**b**), and residual strain (**c**) of the $Cu_{(50-x)}Zr_{50}Al_x$ alloys with Al = 0, 5, 10, 15 at. %. The stresses and strains are compressive.

4. Conclusions

The present work explores the possibility of alloying a binary $Cu_{50}Zr_{50}$ alloy by adding different amounts of Al (5, 10, and 15 at. %) in place of Cu. The presence of aluminum causes a reduction in the proportion of the CuZr phase and the formation of secondary phases (τ5, $CuZr_2$). These microstructural changes strongly influenced the characteristics of MT: while in the binary alloy the transformation is stabilized only after eight thermal cycles, samples containing aluminum exhibit stable MT ab initio. Transformation temperatures and enthalpies get lower as the aluminum content is increased: this effect does not permit any possibilities in the use of these alloys as HTMAs. The Al alloying, in the range from 5% up to 10%, made evident a pseudoelastic behavior under compression, while higher Al content induced high brittleness, in a similar manner to the binary CuZr alloy after MT stabilization.

It can be concluded that Al addition to equiatomic alloy, although it stabilizes the martensitic transformation, does not allow for the use of the alloy as an HTSMA. Further studies on different alloying elements focused on finding a proper balance between thermal cycling stability and suitable high transformation temperatures are required before using a CuZr based system for the development of HTSMA for industrial applications.

Author Contributions: Conceptualization, C.A.B. and A.T.; methodology, C.A.B.; validation, all authors.; formal analysis, C.A.B., J.F. and M.C.; investigation, C.A.B., J.F. and M.C.; resources, A.T.; writing—original draft preparation, C.A.B., J.F. and M.C.; writing—review and editing, all authors; visualization, C.A.B.; supervision, A.T.; project administration, A.T.; funding acquisition, A.T. All authors have read and agreed to the published version of the manuscript.

Funding: This research was funded through Accordo Quadro between CNR and Regione Lombardia, grant number 3866.

Data Availability Statement: Data available on request.

Acknowledgments: The work was developed within the framework of 2° Accordo Quadro CNR/Regione Lombardia. The authors would like to thank Marco Pini, Nicola Bennato, and Giordano Carcano of CNR ICMATE, Lecco Unit, for their technical assistance.

Conflicts of Interest: The authors declare no conflict of interest.

References

1. Otsuka, K.; Wayman, C.M. *Shape Memory Materials*; Cambridge University Press: New York, NY, USA, 1998.
2. Hodgson, D.E. Fabrication, Heat Treatment and Joining of Nitinol Components. In *SMST-2000: Proceedings of the International Conference on Shape Memory and Superelastic Technologies*; ACM: New York, NY, USA, 2001; pp. 11–24.
3. Koval, Y.; Firstov, G.; Kotko, A. Martensitic transformation and shape memory effect in ZrCu intermetallic compound. *Scr. Met. Mater.* **1992**, *27*, 1611–1616. [CrossRef]
4. Schryvers, S.D. TEM investigation of the microstructure and defects of CuZr martensite. Part I: Morphology and twin systems. *Acta Mater.* **1998**, *46*, 1165–1175.
5. Seo, J.W.; Schryvers, D. EM investigation of the microstructure and defects of CuZr martensite. Part II: Planar defects. *Acta Mater.* **1998**, *46*, 1177–1183.
6. Carvalho, E.M.; Harris, I.R. Constitutional and structural studies of the intermetallic phase, ZrCu. *J. Mater. Sci.* **1980**, *15*, 1224–1230. [CrossRef]
7. Biffi, C.; Figini, A.; Tuissi, A. Influence of compositional ratio on microstructure and martensitic transformation of CuZr shape memory alloys. *Intermetallics* **2014**, *46*, 4–11. [CrossRef]
8. Firstov, G.S.; Van Humbeeck, J.; Koval, Y.N. Peculiarities of the martensitic transformation in ZrCu intermetallic compound—potential high temperature SMA. *J. Phys. Colloq.* **2001**, *11*, 481–486. [CrossRef]
9. Biffi, C.; Coduri, M.; Yoshida, H.; Soejima, Y.; Nishida, M.; Tuissi, A. The effect of thermal cycling on the martensitic transformation in equiatomic CuZr shape memory alloy. *J. Alloy. Compd.* **2015**, *653*, 591–595. [CrossRef]
10. Hisada, S.; Matsuda, M.; Nishida, M.; Biffi, C.A.; Tuissi, A. Microstructure and Martensitic Transformation Behavior in Thermal Cycled Equiatomic CuZr Shape Memory Alloy. *Metals* **2019**, *9*, 580. [CrossRef]
11. Song, K.; Pauly, S.; Zhang, Y.; Gargarella, P.; Li, R.; Barekar, N.; Kühn, U.; Stoica, M.; Eckert, J. Strategy for pinpointing the formation of B2 CuZr in metastable CuZr-based shape memory alloys. *Acta Mater.* **2011**, *59*, 6620–6630. [CrossRef]
12. Firstov, G.S.; Van Humbeeck, J.; Koval, Y.N. High-temperature shape memory alloys: Some recent developments. *Mater. Sci. Eng.* **2004**, *378*, 2–10. [CrossRef]

13. Firstov, G.S.; van Humbeeck, J.; Koval, Y.N. Comparison of high temperature shape memory behaviour for ZrCu-based, Ti–Ni–Zr and Ti–Ni–Hf alloys. *Scripta Mater.* **2004**, *50*, 243–248. [CrossRef]
14. Biffi, C.A.; Albisetti, A.F.; Tuissi, A. CuZr Based Shape Memory Alloys: Effect of Cr and Co on the Martensitic Transformation. *Mater. Sci. Forum* **2013**, *738–739*, 167–171. [CrossRef]
15. Koval, Y.; Firstov, G.; Delaey, L.; Humbeeck, J. The influence of Ni and Ti on the martensitic transformation and shape memory effect of the intermetallic compound ZrCu. *Scr. Metall. Mater.* **1994**, *31*, 799–802. [CrossRef]
16. Biffi, C.A.; Tuissi, A. Hot Workability of Cu-Zr Based Shape Memory Alloys for Potential High Temperature Applications. *J. Mater. Eng. Perform.* **2014**, *23–27*, 2379. [CrossRef]
17. Gao, W.; Yi, X.; Song, G.; Wang, Z.; Meng, X. $Zr_{50}Cu_{25}Ni_{7.5}Co_{17.5}$ high-temperature shape memory alloy with excellent thermal stability and large recovery strain, and the associated microstructural deformation mechanism. *Mater. Des.* **2020**, *196*, 109108. [CrossRef]
18. Qiu, F.; Shen, P.; Liu, T.; Lin, Q.; Jiang, Q. Electronic structure and phase stability during martensitic transformation in Al-doped ZrCu intermetallics. *J. Alloy. Compd.* **2010**, *491*, 354–358. [CrossRef]
19. Qiu, F.; Wang, H.; Liu, T.; Jiang, Q. Influence of Al content on the microstructure and mechanical property of the $(Zr_2Cu)_{100-x}Al_x$ alloys. *J. Alloy. Compd.* **2009**, *468*, 195–199. [CrossRef]
20. Meng, F.Q.; Tsuchiya, K.; Yin, F.X.; Li, S.; Yokoyama, Y. Influence of Al content on martensitic transformation behaviour in $Zr_{50}Cu_{50-x}Al_x$. *J. Alloy. Compd.* **2012**, *522*, 136–140. [CrossRef]
21. Gao, W.; Meng, X.; Cai, W.; Zhao, L. ffects of Co and Al addition on martensitic transformation and microstructure in ZrCu-based shape memory alloys. *Trans. Nonferrous Met. Soc. China* **2015**, *25*, 850–855. [CrossRef]
22. Barekar, N.; Gargarella, P.; Song, K.; Pauly, S.; Kühn, U.; Eckert, J. Effect of Al and Ag addition on phase formation, thermal stability, and mechanical properties of Cu–Zr-based bulk metallic glasses. *J. Mater. Res.* **2011**, *26*, 14. [CrossRef]
23. Kwon, O.J.; Kim, Y.C.; Kim, K.B.; Lee, Y.K.; Fleury, E. Formation of amorphous phase in the binary Cu−Zr alloy system. *Met. Mater. Int.* **2006**, *12*, 207–212. [CrossRef]
24. Massalski, T.B.; Okamoto, H.; Subramanian, P.R.; Kacprzak, L. *Binary Alloy Phase*, 2nd ed.; ASM International: Materials Park, OH, USA, 1990.
25. Raghavan, V. Al-Cu-Zr (Aluminum-Copper-Zirconium). *J. Phase Equilibria Diffus.* **2011**, *32*, 452–454. [CrossRef]
26. Wang, C.P.; Tu, S.B.; Yu, Y.; Han, J.J.; Liu, X.J. Experimental investigation of phase equilibria in the Zr-Cu-Al system. *Intermetallics* **2012**, *31*, 1–8. [CrossRef]
27. Albisetti, A.F.; Biffi, C.; Tuissi, A. Synthesis and structural analysis of $Cu_{10}Zr_7$. *J. Alloy. Compd.* **2012**, *544*, 42–45. [CrossRef]